Resonance Frequency Tracking for MEMS Gyroscopes Using Recursive Identification

Federico Morelli, Xavier Bombois, Cécile Pernin, Fabricio Saggin, Anton Korniienko, Kévin Colin, Laurent Bako

Resonance Frequency Tracking for MEMS Gyroscopes Using Recursive Identification*

Federico Morelli[1], Xavier Bombois[1,2], Cécile Pernin[1], Fabricio Saggin[1], Anton Korniienko[1], Kévin Colin[3], and Laurent Bako[1]

[1]Laboratoire Ampère, Ecole Centrale de Lyon, Université de Lyon, Ecully, France
[2]Centre National de la Recherche Scientifique (CNRS), France
[3]Automatic Control, School of Electrical Engineering, KTH, Stockholm, Sweden

September 14, 2021

Abstract

MEMS gyroscopes are generally made up of two resonant systems: the so-called drive and sense modes. It is well known that the drive-mode resonance tracking is crucial to make the device operate accurately. In this paper, we propose an approach based on recursive identification that allows to estimate the resonance frequency over the time. The proposed approach pertains to a recently developed control conguration which is based on the H_∞ control framework.

1 Introduction

In the last years, micro-electro-mechanical (MEMS) inertial sensors have found their way in our daily life. Indeed, most of the smart phones are equipped with accelerometers and gyroscopes to ensure e.g., image stabilization and navigation. The field of application of MEMS inertial sensors is actually much wider. MEMS inertial sensors can indeed also be found in drones and autonomous vehicles, in automotive safety systems, in consumer electronics, in guidance and navigation systems, in numerous industrial applications and in medical devices [1, 10, 21].

In this paper, we are particularly interested in MEMS gyroscopes. A MEMS gyroscope is made up of two proof masses (the so-called drive and sense modes) and allows to determine the angular rate of an object using the principle of the Coriolis force. In order to use this principle, a control system ensures that one of the proof masses (i.e., the drive mode one) vibrates in a controlled way [19]. Indeed, if the latter is done appropriately, the value of the angular rate can be accurately estimated from a measure of the Coriolis force acting the second proof mass (i.e., the sense mode one).

As mentioned above, it is of the utmost importance that the proof mass of the drive mode vibrates in a controlled way. This proof mass is fixed to a reference frame via micro-silicon beams and can be driven via a force. The transfer function between this force u_x and the position x of the mass can generally be accurately represented by a (lightly-damped) second-order resonating system (an extra pole may be necessary to account for the instrumentation). We will call this system the *drive mass system* in the sequel. This drive mass system must thus vibrate in a controlled way.

*The financial support of BPI France (Next4MEMS project) is gratefully acknowledged.

By this, we mean that x must follow a sinusoidal reference signal x_{ref}. Generally, this control objective is achieved via two parallel loops that respectively control the amplitude and the phase of the phasor representation of the to-be-controlled signal x (see e.g. [7]). In [3], an alternative is proposed where the amplitude information of the phasor is used to generate a non-linear oscillator at the resonance frequency. Besides these phasor approaches, the literature also considers techniques that are more classical from a control engineering point-of-view i.e., techniques that compute the control action u_x based on the actual measurement of the position x of the drive mass system (i.e., without having first to transform the signal x into its phasor description). We can distinguish different types of approaches: adaptive control [11, 14, 8], active disturbance rejection [6] and Model Predictive Control [15].

Since the to-be-controlled system can be represented by a third-order linear system[1], the use of classical linear control design methods (such as frequency design methods, H_∞ control, ...) is certainly also another valid option to efficiently control the drive mass system (these techniques indeed easily allow one to enforce stability and performance guarantees). With these control design methods, the force u_x is computed as the output of a linear controller K_x that takes as input the difference[2] between the sinusoidal reference signal x_{ref} and the measurement of the position x of the proof mass of the drive mode. Within these classical linear control design methods, H_∞ control is a particularly promising solution. Indeed, as shown in Chapters 3 and 4 of [16], the H_∞ framework allows one to define the specifications of the controller K_x in order to guarantee an accurate measurement of the angular rate by the MEMS gyroscope. This possibility is the main reason that has led us to consider an H_∞ control approach in the Next4MEMS project, an industrial project which aims at improving the performance of MEMS gyroscopes. Within this project, system identification has been used to derive, using specially dedicated open-loop experiments, accurate models of the dynamics of the gyroscopes (together with its instrumentation) [4]. Based on such an identified model, an H_∞ control approach has been devised in order to design the controller K_x ensuring a sufficiently accurate tracking of the sinusoidal reference x_{ref} for the sensing accuracy of the MEMS gyroscope to be guaranteed [18, 16]. In addition, the frequency of the to-be-tracked sinusoidal reference x_{ref} is chosen equal to the resonance frequency[3] of the identified model of the drive mass system in order to reduce the energy consumption (i.e., to enforce a small actuation signal u_x).

The fact that the controller has to follow a sinusoidal reference signal x_{ref} at the resonance frequency of the drive mass system makes the linear control loop described in the previous paragraph particularly vulnerable to eventual variations of this resonance frequency. Yet, these variations of the resonance frequency are rather frequent. Indeed, it is well known [19] that the value of the resonance frequency of the drive mass system is influenced by a number of factors (such as the ambient temperature), while MEMS gyroscopes have to operate in a large range of external circumstances. In the control configuration based on the phasor description [7, 3], these variations of the resonance frequency are relatively easily taken care of. In particular, in the classical two-loop configuration (see [7]), the phase loop allows a smooth tracking of the resonance frequency since this loop ensures that the phase shift between u_x and x is kept at a value[4] of $\frac{-\pi}{2}$ rad. In the control

[1] As will be discussed in the next paragraph, this will in fact hold for a fixed environment (i.e., temperature, pressure, ...).

[2] In this paper, we will consider a controller with one degree of freedom, but the results also apply to controllers with two degrees of freedom.

[3] Recall that the drive mass system is basically a (lightly-damped) resonating system.

[4] If the drive mass system is a pure resonator, this property can only be attained if u_x and x are sinusoids at the resonance frequency. Note however that, due to the dynamics of the instrumentation, the argument of the frequency response of the drive mass system at the resonance frequency will not be precisely equal to $\frac{-\pi}{2}$ rad.

configuration with a linear controller that we consider in the Next4MEMS project, the variation of the resonance frequency is not dealt with in such an easy way. That is why, in this paper, we propose an approach to make this control configuration able to tackle the resonance frequency variations. For this purpose, we supply this control configuration with an algorithm that estimates the resonance frequency over time. This estimate can then be used to adapt the frequency of the sinusoidal reference signal x_{ref}. The above-mentioned algorithm is based on a recursive identification scheme that allows to follow the evolution of the dynamics of the drive mass system over time and, therefore, also the evolution of its resonance frequency.

To validate our approach, we implement it on the test benchmark platform of the Next4MEMS project where a development kit designed for experimenting new control strategies for MEMS sensors (the AS3125-SDK platform developed by ASYGN) is used in combination with a MEMS gyroscope prototype (see [18]). Using a thermal chamber to enforce fast temperature variations (and thus fast resonance frequency variations), we show that the proposed recursive identification scheme allows to appropriately follow the evolution of the resonance frequency. More importantly, we also show that the performance of the closed loop made up of the drive mass system and of a linear controller[5] K_x is strongly improved when we adapt the frequency of the sinusoidal reference x_{ref} based on this estimate of the resonance frequency (compared to the case where this is not done).

Notations: The matrix I_n denotes the identity matrix of dimension n. The symbol z will not only represent the Z-transform variable, but also the shift operator. For a discrete-time signal $x(t)$, t represents the sample number. Finally, $\mathbb{R}$ denotes the set of real numbers.

2 Description of the drive mass system and of its control system

2.1 Identified model of the drive mass system

As mentioned in the introduction, the resonance frequency of the drive mass system G_x can vary due to a number of factors among which temperature variation is the most important one. In this paper, we will present a methodology allowing to adapt the sinusoidal reference signal x_{ref} of the closed loop represented in Figure 1 in order to maintain its performance level despite these possible variations of the resonance frequency. The controller K_x of this closed loop is here designed based on a nominal model $\hat{G}_x$ of G_x that is identified using the open-loop prediction error procedure presented in Chapter 7 of [4]. It is important to stress that this nominal model will only accurately represent the drive mass system when the factors influencing the resonance frequency will be close to the ones observed during the identification experiment. As an example, the ambient temperature at which the experiment has been performed was 30 ^oC (in the sequel, we will call this temperature the nominal temperature T_{nom}). The identification procedure at T_{nom} has led to the following (discrete-time) model of the drive mass system (the sampling time T_s is here equal to 1.6 10^{-5} s):

$$x(t) = \underbrace{\hat{G}_x(z)\ u_x(t)}_{\breve{x}(t)} + \underbrace{\hat{H}_x(t)\ e_x(t)}_{v_x(t)} \tag{1}$$

where u_x is the force applied to the drive mass system (i.e., the input[6] of the drive mass system), x is the position of the drive mass (i.e., the output of the drive mass system) and v_x the process

[5] This linear controller will be here an H_∞ controller.

[6] The actuation system is in fact a bit more complex: the force u_x is indeed generated via a voltage source (see e.g., [4]).

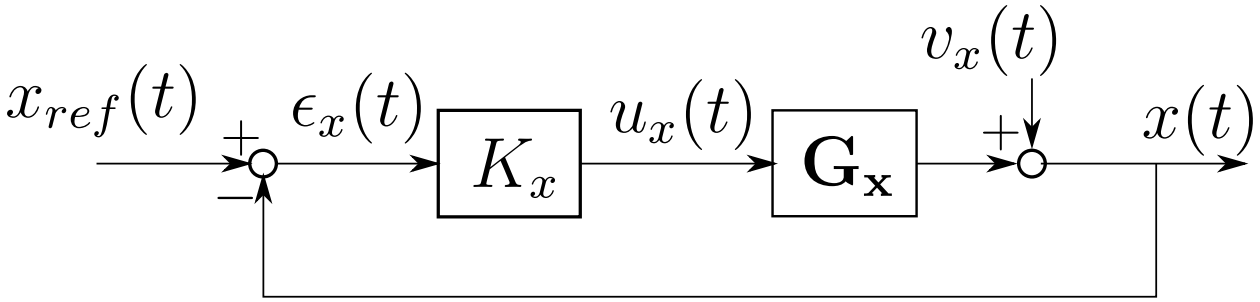

Figure 1: Schematic of the control strategy of the drive mass system.

noise acting on the drive mass system. The plant transfer function model $\hat{G}_x(z)$ is given by

$$\hat{G}_x(z) = \frac{b_1 z^{-1} + b_2 z^{-2} + b_3 z^{-3}}{1 + f_1 z^{-1} + f_2 z^{-2} + f_3 z^{-3}} \tag{2}$$

with $b_1 = -8.508\ 10^{-6}$, $b_2 = -2.576\ 10^{-5}$, $b_3 = -5.439\ 10^{-6}$, $f_1 = -1.189$, $f_2 = 1.315$ and $f_3 = -0.3988$. The process noise v_x is modeled as $\hat{H}_x(t)e_x(t)$ with a white noise e_x of variance $\sigma_e^2 = 2.97\ 10^{-6}$ and with:

$$\hat{H}_x(z) = \frac{1 + c_1 z^{-1} + c_2 z^{-2} + c_3 z^{-3} + c_4 z^{-4}}{1 + d_1 z^{-1} + d_2 z^{-2} + d_3 z^{-3} + d_4 z^{-4} + d_5 z^{-5}} \tag{3}$$

with $c_1 = 0.9636$, $c_2 = -0.3466$, $c_3 = -1.197$, $c_4 = -0.3669$, $d_1 = -0.05898$, $d_2 = -0.8191$, $d_3 = -0.5455$, $d_4 = 0.5646$ and $d_5 = -0.1345$. The modulus of the frequency responses of $\hat{G}_x$ and $\hat{H}_x$ are given in Figure 2. As mentioned in the introduction, $\hat{G}_x$ is basically a resonating system with a sharp resonance peak (an extra pole is due to the instrumentation). Since a resonating system can be better understood in the continuous time, let us consider the following continuous-time version of the discrete-time transfer function $\hat{G}_x(z)$:

$$\tilde{G}_x(s) = \frac{k}{(\frac{s^2}{\omega_{n,x}^2} + \frac{2\xi}{\omega_{n,x}} s + 1)(\frac{s}{k_f} + 1)} \tag{4}$$

with s the Laplace variable. In this equation, the resonator is described by its (very low) damping ratio $\xi = 5.9\ 10^{-6}$ and its natural frequency $\omega_{n,x} = 72788.728866\ rad/s$, while $k = -5.46\ 10^{-5}$ is the static gain of the transfer function and $k_f = 5.7\ 10^4$ represents the extra pole due to the instrumentation. The resonance frequency of $\tilde{G}_x(s)$ (and of $\hat{G}_x(z)$) is defined as the frequency $\omega_{r,x}$ at which the modulus $|\tilde{G}_x(j\omega)|$ of the frequency response of $\tilde{G}_x$ is the largest i.e., $\omega_{r,x} = 72788.728864\ rad/s$. This frequency is extremely close to the natural frequency $\omega_{n,x}$ due to the low damping ratio ξ and can be deduced[7] as $\omega_{r,x} = \omega_{n,x}\sqrt{1 - 2\xi^2}$. For further reference, the resonance frequency $\omega_{r,x} = 72788.728864\ rad/s$ will be denoted $\omega_{r,x}^{nom}$ since it is the resonance frequency of the nominal model.

The modulus $|\hat{H}_x(e^{j\omega T_s})|$ of the frequency response of the noise transfer function $\hat{H}_x$ presents higher gains in low frequencies than in high frequencies. Observe also the resonance peak at a frequency which is slightly higher than $\omega_{r,x}^{nom}$ (see Figure 2b).

[7]This relation is in fact a (small) approximation since this relation is only valid for a second-order resonator.

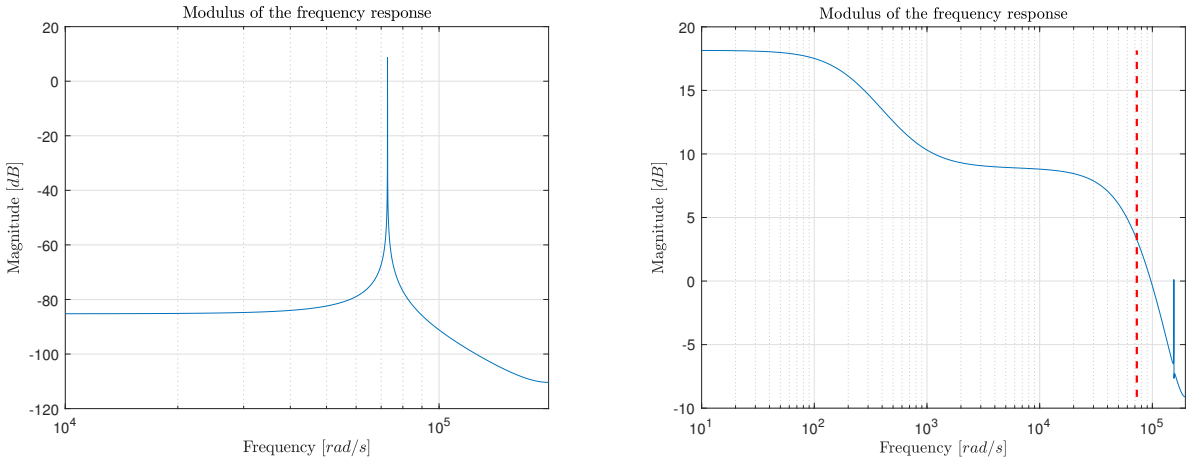

(a) $\left|\hat{G}_x(e^{j\omega T_s})\right|$ (b) $\left|\hat{H}_x(e^{j\omega T_s})\right|$

Figure 2: Modulus of the frequency responses of $\hat{G}_x$ (blue line in plot (a)) and of $\hat{H}_x$ (blue line in plot (b)). The vertical line in red dashed is placed at $\omega = \omega_{r,x}^{nom}$ in plot (b).

2.2 Closed-loop system and nominal performance

As mentioned in Section 1, the drive mass system is operated in closed loop to generate and ensure a sinusoidal oscillation of the mass. For this purpose, we will use the following control configuration using a linear time-invariant (LTI) controller $K_x(z)$ (see also Figure 1):

$$\begin{cases} x(t) = G_x(z)u_x(t) + v_x(t) \\ u_x(t) = K_x(z)\ \epsilon_x(t) \\ \epsilon_x(t) = x_{ref}(t) - x(t) \end{cases} \tag{5}$$

where the reference signal $x_{ref}(t)$ is chosen as

$$x_{ref}(t) = A_x \sin\left(\omega_{ref}\ t\ T_s\right) \tag{6}$$

with A_x the desired amplitude of the oscillation ($A_x = 0.5$ in our case) and ω_{ref} the desired frequency of the oscillation. To limit the control action, ω_{ref} has to be chosen as close as possible to the resonance frequency of the actual drive mass system G_x. At nominal temperature[8] T_{nom}, a sensible choice is thus $\omega_{ref} = \omega_{r,x}^{nom}$ i.e., the resonance frequency of the identified model $\hat{G}_x$ of G_x. The controller K_x must be designed in such a way that the tracking of x_{ref} is accurate enough for the sensing objective of the MEMS gyroscope. As shown in Chapter 3 of [16], the design, based on the nominal model (1), of such a controller K_x can be formulated as a convex optimization problem involving an H_∞ criterion [16, 18]. Using this methodology, we here obtain:

$$K_x(z) = \frac{0.1245 - 0.09834\ z^{-1} - 3.88\ 10^{-5}\ z^{-2} + 0.09834\ z^{-3} - 0.1244\ z^{-4}}{1 - 1.578\ z^{-1} + 2.617\ z^{-2} - 1.574\ z^{-3} + 0.9947 z^{-4}} \tag{7}$$

whose modulus of the frequency response is represented in Figure 3. In this figure, we observe the high gain characteristic at $\omega = \omega_{r,x}^{nom}$ (allowing accurate tracking of a sinusoidal reference at this frequency). Note that this high gain characteristic also allows the rejection of the components of the process noise v_x around $\omega = \omega_{r,x}^{nom}$. Note that a better disturbance rejection is here not possible

[8] and when the other external factors influencing the resonance frequency (such as the pressure) are also equal or close to the ones observed during the identification experiment leading to the nominal model (1).

since $\hat{G}_x$ has negligible gains at other frequencies.

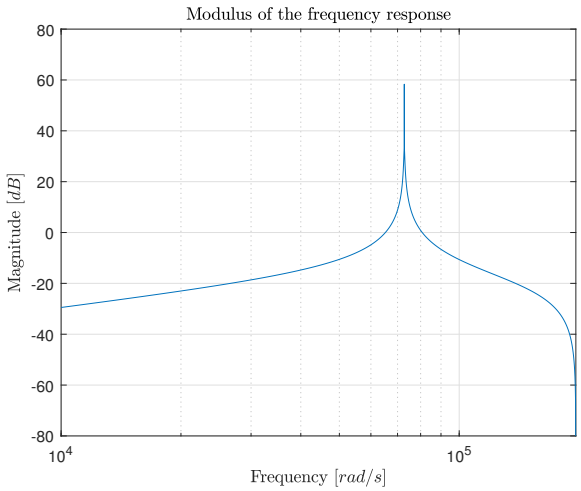

Figure 3: Modulus of the the frequency response of $K_x(z)$

Let us analyze the performance of this controller K_x when applied to the model (1) and when $x_{ref}(t) = A_x \sin(\omega_{r,x}^{nom} t T_s)$ (i.e., the nominal performance of K_x). For this purpose, let us consider the following (nominal) closed-loop transfer functions:

$$S(z) = \frac{1}{1 + \hat{G}_x(z)K_x(z)} \quad , \quad F(z) = \frac{K_x(z)}{1 + \hat{G}_x(z)K_x(z)} \tag{8}$$

In the loop represented in Figure 1 with G_x replaced by $\hat{G}_x$, these transfer functions (whose frequency responses are represented in Figures 4 and 5) relate the external signals x_{ref} and v_x to the tracking error $\epsilon_x = x_{ref} - x$ and the actuation signal u_x, respectively:

$$\epsilon_x(t) = S(z)x_{ref}(t) - S(z)v_x(t) \quad \text{and} \quad u_x(t) = F(z)x_{ref}(t) - F(z)v_x(t) \tag{9}$$

We observe that the modulus of the frequency response of the sensitivity function S is very low ($-67dB$) at $\omega = \omega_{r,x}^{nom}$. This will allow an accurate tracking of x_{ref} and the rejection of the component of the noise v_x around the resonance frequency. We also observe that the transfer function F has a local minimum at $\omega = \omega_{r,x}^{nom}$ ($|F(e^{j\omega_{r,x}^{nom}T_s})| = -8.7dB$). Consequently, the tracking of x_{ref} and the rejection of the component of the noise v_x around the resonance frequency will be achieved with low control efforts.

Let us give more details on the performance of this nominal loop using (9). The signal ϵ_x will be made up of a sinusoidal term of amplitude $A_x|S(e^{j\omega_{r,x}^{nom}T_s})| = A_x/2238 = 2\ 10^{-4}$ and a Gaussian noise contribution of standard deviation $||H_xS||_2\sigma_e = 0.0027$ (the 2-norm $||H_xS||_2$ of H_xS is indeed equal to 1.57). This Gaussian noise contribution will therefore be the dominant part of ϵ_x.

As far as u_x is concerned, we observe that $||H_xF||_2 = 3.64$. Consequently, u_x is made up of a sinusoidal part of amplitude $A_x|F(e^{j\omega_{r,x}^{nom}T_s})| = 0.37A_x = 0.185$ and a Gaussian noise contribution of standard deviation $||H_xF||_2\sigma_e = 0.033$.

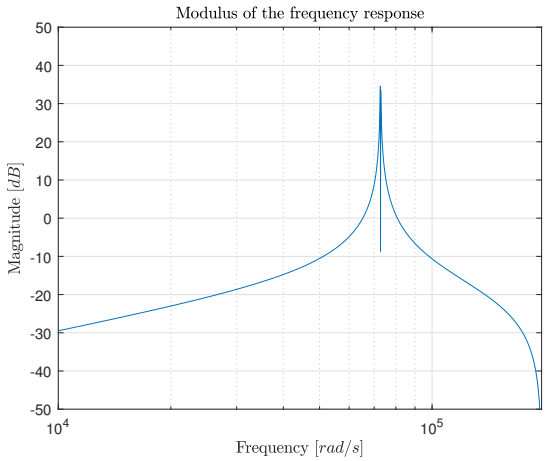

(a) $\left|F(e^{j\omega T_s})\right|$

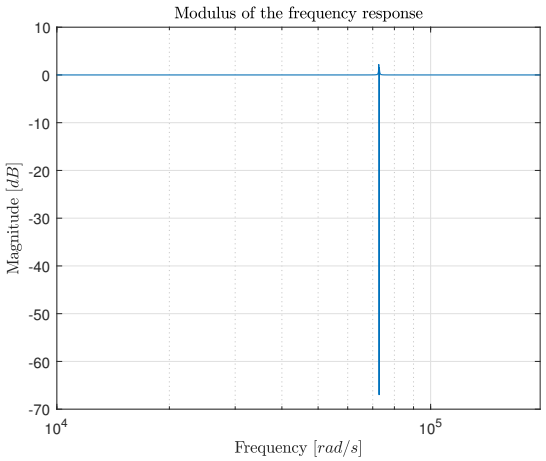

(b) $\left|S(e^{j\omega T_s})\right|$

Figure 4: Modulus of the frequency responses of $F(z)$ (blue line in plot (a)) and of $S(z)$ (blue line in plot (b)).

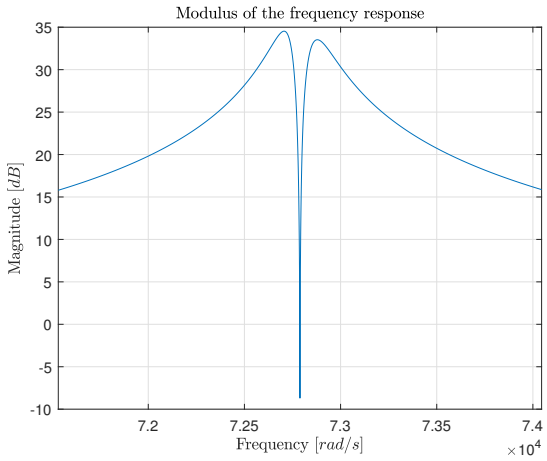

(a) $\left|F(e^{j\omega T_s})\right|$

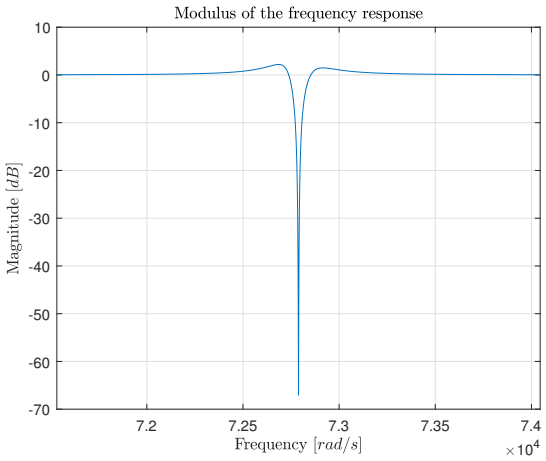

(b) $\left|S(e^{j\omega T_s})\right|$

Figure 5: Zoom of Figure 4 around $\omega = \omega_{r,x}^{nom}$. The downward peaks observed in these figures are located at $\omega = \omega_{r,x}^{nom}$.

These observations are confirmed by the following simulation. The loop in Figure 1 is simulated for 70 seconds[9] with the nominal model (1) and with the controller K_x given in (7) and using $x_{ref}(t) = 0.5\sin(\omega_{r,x}^{nom} t T_s)$. In Figure 6, we give the obtained signals ϵ_x and u_x.

Since they have been obtained on the closed loop made up of the nominal model (1) and of the controller K_x designed with that model, the signals given in Figure 6 are representative of the desired level of performance (i.e., the *nominal performance*). In particular, an actuation signal u_x of (maximal) amplitude 0.2 and a tracking error ϵ_x of (maximal) amplitude 0.015 will therefore be seen as *good* performance. Consequently, if such amplitudes are also observed when the loop is perturbed by a varying resonance frequency, we will then be able to conclude that the nominal performance is maintained despite the varying resonance frequency.

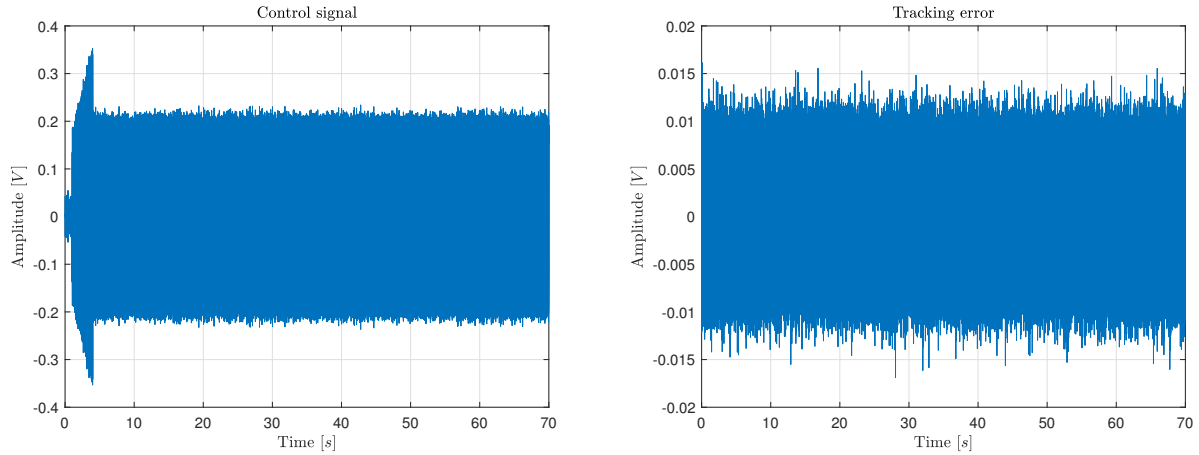

(a) u_x (b) ϵ_x

Figure 6: Results of the simulation described in Section 2.2 (nominal performance).

2.3 Influence of resonance frequency variations on the performance

In this subsection, we will analyze the performance of the loop represented in Figure 1 when the resonance frequency of G_x varies. These variations are indeed very frequent in practice [19]. As an example, we typically observe that, in steady state, the resonance frequency is decreased by 1 rad/s when the temperature is increased by 1 ^oC.

Let us thus simulate the loop represented in Figure 1 using the controller K_x designed with the nominal model (see (7)) and the sinusoidal reference at the frequency of the nominal model (i.e. $x_{ref}(t) = 0.5\sin(\omega_{r,x}^{nom} t T_s)$), but with the resonance frequency of G_x that varies as follows (see also Figure 7):

$$\omega_{r,x}(t) = \begin{cases} \omega_{r,x}^{nom} & tT_s \leq 75 \\ \omega_{r,x}^{nom} + \alpha_\omega (tT_s - 75) & 75 < tT_s \leq 575 \\ \omega_{r,x}^{nom} + 500\alpha_\omega & 575 < tT_s \leq 675 \end{cases} \tag{10}$$

with $\alpha_\omega = 0.0804$ i.e., the resonance frequency changes from $\omega_{r,x}^{nom} = 72788$ rad/s to 72828 rad/s

[9] In this simulation, during the first four seconds, the amplitude A_x of x_{ref} is progressively increased from zero to 0.5. This is done in order to limit the transient behaviour.

in 500 seconds.

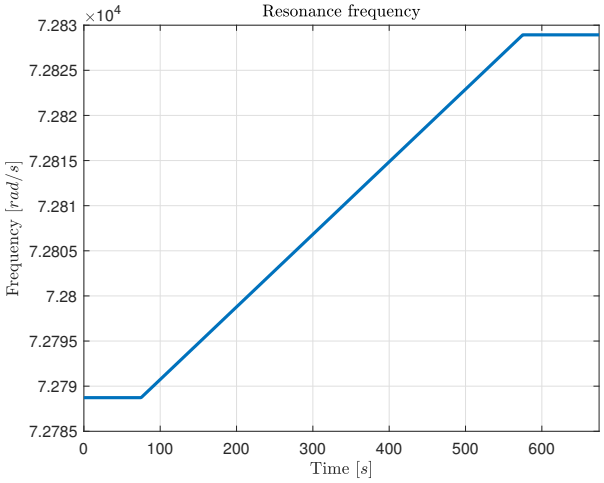

Figure 7: Varying resonance frequency as given by (10)

Under the circumstances given in (10), the signals ϵ_x and u_x describing the performance of the closed-loop system of Figure 1 are given by the blue curves in Figure 8. Comparing these signals with the ones in Figure 6, it is clear that the amplitudes of both signals are much higher once the resonance frequency is no longer equal to $\omega_{r,x}^{nom}$ (i.e., after 75 seconds). In other words, the performance of the closed loop is strongly altered[10] when the resonance frequency is no longer equal to $\omega_{r,x}^{nom}$.

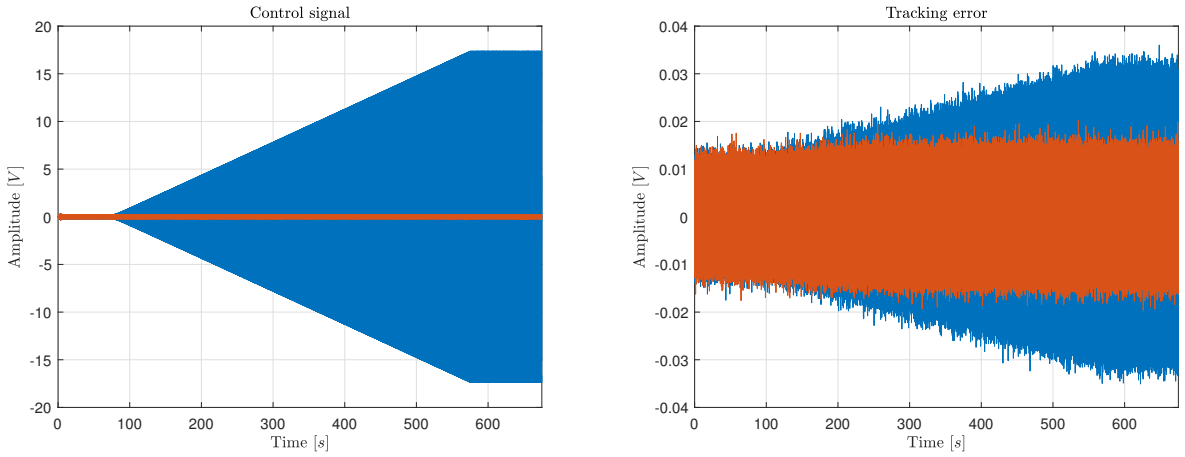

(a) u_x. (b) ϵ_x.

Figure 8: Results of the simulations described in Sections 2.3 and 2.4 with a varying resonance frequency given by (10). The blue curve corresponds to the case where $x_{ref}(t) = 0.5\sin(\omega_{r,x}^{nom} t T_s)$ and the red curve corresponds to the case where x_{ref} is given by (15) with $\omega_{ref}(t) = \omega_{r,x}(t)$

In order to perform the simulation with the varying resonance frequency (10), the closed-loop system in Figure 1 is simulated using the following Linear Parameter Varying operator to

[10] An eventual saturation of u_x could lead to a signal ϵ_x with an even higher amplitude.

compute $x(t)$:

$$\begin{cases} \mathbf{G_x}(\omega_{r,x}(t)) \ : \ \breve{x}(t) = b_1(\omega_{r,x}(t))u_x(t-1) + b_2(\omega_{r,x}(t))u_x(t-2) + b_3(\omega_{r,x}(t))u_x(t-3)\ldots \\ \qquad \cdots - f_1(\omega_{r,x}(t))\breve{x}(t-1) - f_2(\omega_{r,x}(t))\breve{x}(t-2) - f_3(\omega_{r,x}(t))\breve{x}(t-3) \\ x(t) = \breve{x}(t) + v_x(t) \end{cases} \tag{11}$$

where the time-varying coefficients $b_i(\omega_{r,x}(t))$ and $f_j(\omega_{r,x}(t))$ $(i = 1, ..., 3,\ j = 1, ..., 3)$ at time t are determined as the coefficients of the discrete-time version $\mathbf{G_x}(z, \omega_{r,x})$ of the following continuous-time transfer function with $\omega_{r,x}$ equal to the value of $\omega_{r,x}(t)$ at time t:

$$\tilde{\mathbf{G}}_{\mathbf{x}}(s, \omega_{r,x}) = \frac{k}{\left(\frac{1-2\xi^2}{\omega_{r,x}^2}s^2 + \frac{2\xi\sqrt{1-2\xi^2}}{\omega_{r,x}}s + 1\right)\left(\frac{s}{k_f} + 1\right)} \tag{12}$$

where $\xi = 5.9\ 10^{-6}$, $k = -5.46\ 10^{-5}$ and $k_f = 5.7\ 10^4$ (such as in (4)). The discrete-time version of (12) has indeed the following form:

$$\mathbf{G_x}(z, \omega_{r,x}) = \frac{b_1(\omega_{r,x})z^{-1} + b_2(\omega_{r,x})z^{-2} + b_3(\omega_{r,x})z^{-3}}{1 + f_1(\omega_{r,x})z^{-1} + f_2(\omega_{r,x})z^{-2} + f_3(\omega_{r,x})z^{-3}} \tag{13}$$

The modulus of the frequency response of $\mathbf{G_x}(z, \omega_{r,x})$ for different frozen values of $\omega_{r,x}$ in the interval $[72748 \quad 72828]\ rad/s$ are represented in Figure 9.

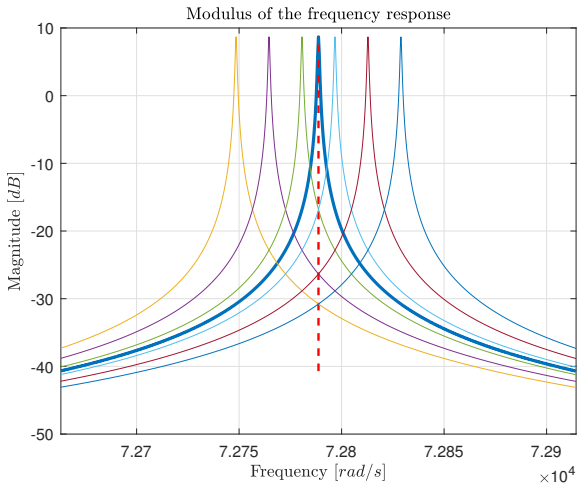

Figure 9: $\left|\mathbf{G_x}(e^{j\omega T_s}, \omega_{r,x})\right|$ for different frozen values of $\omega_{r,x} \in [72748 \quad 72828]\ rad/s$. The tick blue line represents this modulus for $\omega_{r,x} = \omega_{r,x}^{nom}$. The vertical line in red dashed is placed at $\omega = \omega_{r,x}^{nom}$.

In order to understand the performance degradation observed in Figure 8, it is useful to observe the frequency response of the following closed-loop transfer functions:

$$S_{\omega_{r,x}}(z) = \frac{1}{1 + \mathbf{G_x}(z, \omega_{r,x})K_x(z)} \quad F_{\omega_{r,x}}(z) = \frac{K_x(z)}{1 + \mathbf{G_x}(z, \omega_{r,x})K_x(z)} \tag{14}$$

that corresponds to a loop made up of the controller K_x (see (7)) and the plant $\mathbf{G_x}(z, \omega_{r,x})$ i.e., a plant with a resonance at a frequency $\omega_{r,x}$. The modulus of the frequency responses of these

two transfer functions are represented in Figure 10 for different values of $\omega_{r,x} \in [72748 \quad 72828]$ rad/s. Let us observe that the moduli of the frequency response of these transfer functions evaluated at $\omega = \omega_{r,x}^{nom}$ (i.e., $\left|F_{\omega_{r,x}}(e^{j\omega_{r,x}^{nom}T_s})\right|$ and $\left|S_{\omega_{r,x}}(e^{j\omega_{r,x}^{nom}T_s})\right|$) are much larger when these transfer functions are computed with a plant $\mathbf{G_x}(z, \omega_{r,x})$ with a resonance frequency $\omega_{r,x} \neq \omega_{r,x}^{nom}$ than when they are computed with the nominal model considered in the previous subsection i.e., $\mathbf{G_x}(z, \omega_{r,x}^{nom}) \triangleq \hat{G}_x(z)$. This larger modulus is the main reason of the performance degradation observed in Figure 8 (recall that $x_{ref}(t) = 0.5\sin(\omega_{r,x}^{nom} t T_s)$ in this simulation). Note indeed that $||H_x F_{\omega_{r,x}}||_2$ and $||H_x S_{\omega_{r,x}}||_2$ remain (approximatively) equal to 3.64 and 1.57, when $\omega_{r,x}$ varies in $[72748 \quad 72828]$ rad/s.

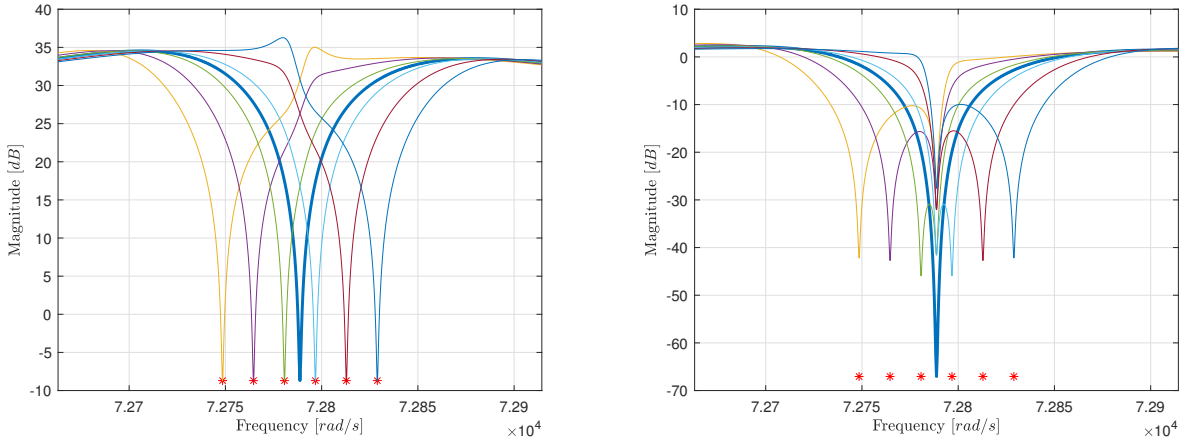

(a) $\left|F_{\omega_{r,x}}(e^{j\omega T_s})\right|$ (b) $\left|S_{\omega_{r,x}}(e^{j\omega T_s})\right|$

Figure 10: Modulus of the frequency responses of the two transfer functions in (14) for different values of $\omega_{r,x} \in [72748 \quad 72828]$ rad/s. The tick blue line in both plots represents the modulus for $\omega_{r,x} = \omega_{r,x}^{nom}$. For the transfer functions with $\omega_{r,x} \neq \omega_{r,x}^{nom}$, the red asterisks are located at $\omega = \omega_{r,x}$ in each of these plots.

2.4 Proposed approach to tackle the variations of the resonance frequency of the drive mass system

Figure 10 also allows to justify the procedure proposed in the introduction to tackle the resonance frequency variations. Let us indeed observe that $\left|F_{\omega_{r,x}}(e^{j\omega T_s})\right|$ and $\left|S_{\omega_{r,x}}(e^{j\omega T_s})\right|$ both present a minimum at $\omega = \omega_{r,x}$. Consequently, when the plant presents a resonance at $\omega_{r,x}$, the closed loop made up of this plant and the controller K_x (see (7)) will be able to track a sinusoidal reference at that particular frequency $\omega_{r,x}$ (i.e., $x_{ref}(t) = 0.5\sin(\omega_{r,x} t T_s)$) with a small tracking error ϵ_x and a small u_x. Consequently, as proposed in the introduction, the resonance frequency variations will be here tackled by just adapting x_{ref}, while letting the linear time-invariant controller K_x unchanged.

The above reasoning is done for a frozen value of the resonance frequency. Extending this reasoning to the case of a resonance frequency $\omega_{r,x}(t)$ varying with time (e.g., as in (10)), we propose the scheme depicted in Figure 11 where $\mathbf{G_x}$ is the LPV operator (11) and where the

reference signal is chosen as:

$$x_{ref}(t) = A_x \sin\left(\sum_{\tau=1}^{t} \omega_{ref}(\tau)\ T_s\right) \tag{15}$$

with $\omega_{ref}(t) = \omega_{r,x}(t)$ (see Figure 11).

When simulating the loop of Figure 11 with the resonance frequency variation given in (10), we obtain the signals ϵ_x and u_x depicted in red in Figure 8. The amplitudes of these signals are very close to the ones observed in the nominal case[11] (see Figure 6), showing the potential efficiency of the proposed approach.

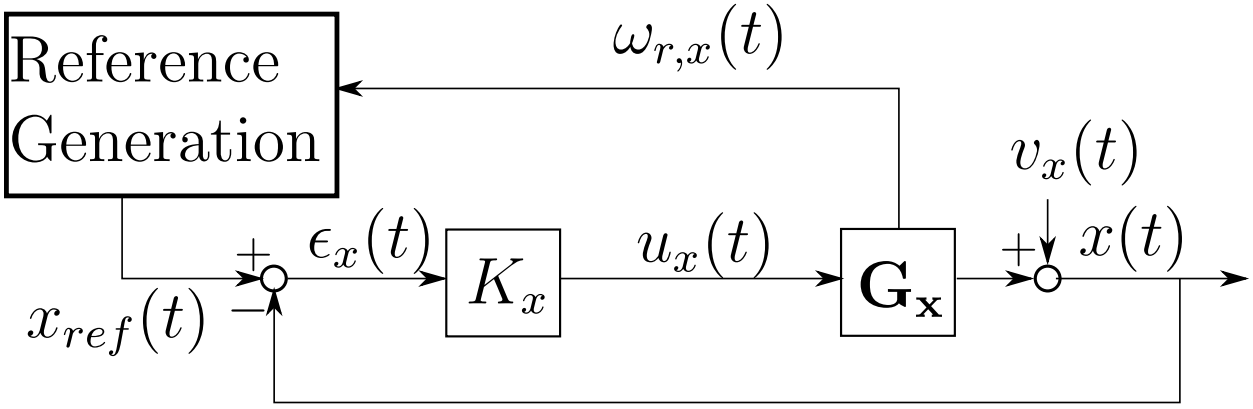

Figure 11: Control of the drive mass system for time varying resonance frequency $\omega_{r,x}(t)$. In this figure, $\mathbf{G_x}$ is the LPV operator (11).

The configuration presented in Figure 11 is however an ideal scenario. Indeed, in practice, the evolution of the resonance frequency over time is unknown and therefore needs to be estimated. As mentioned in the introduction, we propose a recursive identification scheme for this purpose which will yield an estimate $\hat{\omega}_{r,x}(t)$ of $\omega_{r,x}(t)$ and the sinusoidal reference signal (15) will consequently be constructed using $\omega_{ref}(t) = \hat{\omega}_{r,x}(t)$.

Remark. It is to be noted that, to perform the simulations leading to Figure 8, we assume that the only varying parameter of G_x is the resonance frequency while ξ, k and k_f remain equal to the values they had in the nominal model (4). It is important to stress that this assumption is made here only to be able to perform the simulations leading to Figure 8 and that this assumption will not be made in the sequel of the paper. Indeed, even though the resonance frequency is likely to be the parameter that varies most, it is clear that some of the other parameters can also vary with time.

3 Recursive estimation of the varying resonance frequency

3.1 Recursive Identification

Considering the fact that the dynamics of the drive-mass system will vary with external factors (such as the temperature, the pressure, ...) and considering the order of the nominal model of

[11] We nevertheless observe a small increase of the amplitude of ϵ_x. This phenomenon could be expected by comparing the value of $\left|S_{\omega_{r,x}}(e^{j\omega_{r,x}T_s})\right|$ for $\omega_{r,x} \neq \omega_{r,x}^{nom}$ and for $\omega_{r,x} = \omega_{r,x}^{nom}$ in Figure 10b.

this system (see Section 2.1), we can assume the following time-varying model structure for the dynamics of the drive mass system[12]:

$$\begin{cases} \breve{x}(t) = b_{0,1}(t)u_x(t-1) + b_{0,2}(t)u_x(t-2) + b_{0,3}(t)u_x(t-3)\dots \\ \qquad \cdots - f_{0,1}(t)\breve{x}(t-1) - f_{0,2}(t)\breve{x}(t-2) - f_{0,3}(t)\breve{x}(t-3) \\ x(t) = \breve{x}(t) + v_x(t) \end{cases} \tag{16}$$

where $\theta_0(t) = (b_{0,1}(t), b_{0,2}(t), b_{0,3}(t), f_{0,1}(t), f_{0,2}(t), f_{0,3}(t))^T$ is the time-varying parameter vector of dimension $n = 6$. Recursive identification is an identification technique that allows to derive models of time-varying systems such as the one given in (16) via the determination at each time instant of an estimate $\hat{\theta}(t)$ of its time-varying parameter vector $\theta_0(t)$. From this time-varying model $\hat{G}_x(t)$, we will be able to derive an estimate $\hat{\omega}_{r,x}(t)$ of the resonance frequency $\omega_{r,x}(t)$ (which will then be used to adapt the sinusoidal reference x_{ref} of the closed loop made up of the drive mass system and the controller K_x). As we will see in the sequel, at each time instant t, this estimate $\hat{\omega}_{r,x}(t)$ will be given by the resonance frequency of the transfer function that can be obtained if we freeze the coefficients of the time-varying operator $\hat{G}_x(t)$ at their value at time t.

Note that, unlike in the simulations of the previous section, the time-varying model structure (16) does not impose that the resonance frequency is the only parameter that varies over time. It only assumes that the order of the dynamics of the drive mass system will not change over time.

Like in all identification methods, we will need to excite the system with an external signal $r(t)$ in order to guarantee that $\hat{\theta}(t)$ is an accurate estimate of $\theta_0(t)$ (and consequently in order to guarantee that $\hat{\omega}_{r,x}(t)$ is an accurate estimate of $\omega_{r,x}(t)$). This external excitation signal will be denoted $r(t)$ and will be added at the output of the controller K_x (as shown in the bottom of Figure 12):

$$u_x(t) = K_x(z)\left(x_{ref}(t) - x(t)\right) + r(t) \tag{17}$$

In our implementation, $r(t)$ will be chosen as an RBS (Random Binary Sequence) signal of amplitude 0.02 (which is small with respect to the amplitude of the signal u_x observed in Figures 6 and 8).

Let us first present the methodology we have used to determine $\hat{\theta}(t)$ using the measurements of $u_x(t)$ and $x(t)$ obtained in the loop represented in (the bottom of) Figure 12. Among the possible recursive identification algorithms, we have had to make a choice that allowed a compromise between the accuracy of the estimate and the numerical complexity (the currently available electronic card has some strong computational limitations). Based on these considerations, we opted for an Output Error (OE) version of a technique called Recursive Prediction Error (RPE) [12]. As such, this OE version neglects the coloring of the process noise $v_x(t)$ and can therefore lead to biased estimates since the identification is performed under closed-loop operation [12]. However, this bias is likely to be small since the identification is here performed under favorable signal-to-noise ratio ($x(t)$ will be of amplitude 0.5 and $v_x(t)$ has a standard deviation of 0.0027). In the RPE algorithm, the estimate $\hat{\theta}(t)$ at time t is determined by updating the previous value of the estimate (i.e., $\hat{\theta}(t-1)$) using uniquely the output measurement $x(t)$ at time t and the input measurement $u_x(t-1)$ at time $t-1$ and using other quantities that are also recursively updated. In particular, we have[13]:

$$\hat{\theta}(t) = \hat{\theta}(t-1) + R^{-1}(t)\ \psi(t)\ \left(x(t) - \hat{x}(t)\right) \tag{18}$$

[12]The complexity of this model structure can be further reduced by imposing $b_{0,3}(t) = 0$. Indeed, such a model reduction does not influence the accuracy of the estimate $\hat{\omega}_{r,x}(t)$.

[13]In order to reduce the numerical complexity, the inversion of the matrix $R(t)$ in (18) can be easily circumvented (see e.g., [13, pp. 328]).

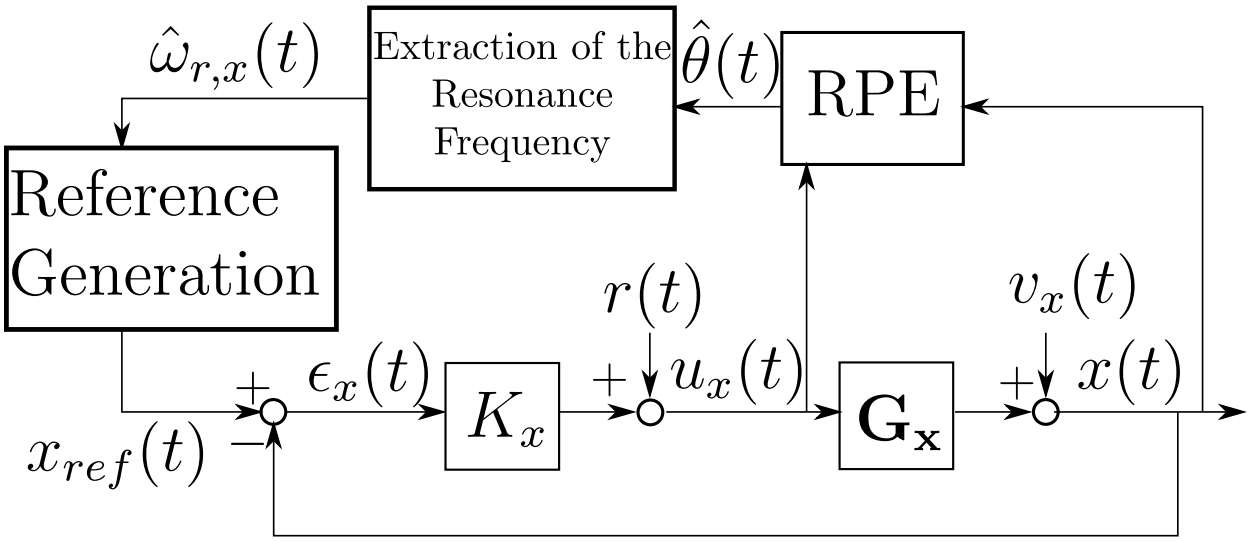

Figure 12: Control of the drive mass system with the estimate $\hat{\omega}_{r,x}(t)$ of the resonance frequency $\omega_{r,x}(t)$ obtained with the Recursive Prediction Error algorithm.

where $x(t)$ is the output measurement at time t and $R(t) \in \mathbb{R}^{n\times n}$, $\psi(t) \in \mathbb{R}^{n\times 1}$ and $\hat{x}(t) \in \mathbb{R}$ are additional quantities that are recursively determined. The quantities $\hat{x}(t)$ and $\psi(t)$ can be determined using $\hat{\theta}(t-1)$ and the input measurement $u_x(t-1)$ at time $t-1$ via the following time-varying state-space representation (the state vector $\varphi(t)$ of this state-space representation is thus also recursively updated):

$$\begin{cases} \varphi(t) = \mathcal{A}(\hat{\theta}(t-1))\ \varphi(t-1)\ +\ \mathcal{B}(\hat{\theta}(t-1))\ u_x(t-1) \\ \begin{pmatrix} \hat{x}(t) \\ \psi(t) \end{pmatrix} = \mathcal{C}(\hat{\theta}(t-1))\ \varphi(t) \end{cases} \tag{19}$$

where, for any value of $\theta = (b_1, b_2, b_3, f_1, f_2, f_3)^T$, $(\mathcal{A}(\theta),\ \mathcal{B}(\theta), \mathcal{C}(\theta))$ is a state-space representation of the following vector of transfer function[14]:

$$\begin{pmatrix} G(z,\theta) \\ \frac{\partial G(z,\theta)}{\partial \theta} \end{pmatrix} \quad \text{with} \quad G(z,\theta) = \frac{b_1 z^{-1} + b_2 z^{-2} + b_3 z^{-3}}{1 + f_1 z^{-1} + f_2 z^{-2} + f_3 z^{-3}} \tag{20}$$

Finally, the matrix $R(t)$ is determined from $R(t-1)$ using the quantity $\psi(t)$ determined in (19):

$$R(t) = \lambda\ R(t-1)\ +\ \psi(t)\psi^T(t) \tag{21}$$

where λ is a scalar tuning parameter, the so-called forgetting factor ($0 < \lambda \leq 1$). This parameter is determined by the user based on the assumed rate of variation of $\theta_0(t)$ in order to optimize the bias-variance trade-off of the estimate. In a nutshell, the faster $\theta_0(t)$ varies, the smaller λ has to be chosen. Here, using a trial-and-error approach, we have determined that $\lambda = 1 - 2\ 10^{-5}$ is a reasonable value.

Once initialized, the recursive algorithm can thus be easily implemented. For this initialization, we have here chosen $\hat{\theta}(0)$ as the parameter vector of the nominal model of the drive mass system i.e., the model identified at nominal temperature and that has been used to design the controller K_x.

[14]It is thus clear that $\hat{x}(t)$ represents the Output Error predictor of $x(t)$ and $\psi(t)$ its gradient.

The other quantities that are recursively updated are initialized as follows $\hat{x}(0) = 0$, $\psi(0) = 0$ and $R(0) = 0.01\ I_n$ (see [13, pp. 299-302] for more details on this choice). Additional features can also be added to the algorithm. It is indeed highly recommended [12, pp. 373] to check at each time instant t if the transfer function $G(z, \theta)$ for $\theta = \hat{\theta}(t)$ is stable and, if it is not the case, to replace (18) by $\hat{\theta}(t) = \hat{\theta}(t-1)$. In addition, it may also be wise to regularly re-initialize the recursive algorithm to avoid numerical issues (that can take the form of an estimate $\hat{\theta}(t)$ that remain constant while $\theta_0(t)$ varies).

3.2 Estimation of the varying resonance frequency using $\hat{\theta}(t)$

Let us now show how we can derive $\hat{\omega}_{r,x}(t)$ from $\hat{\theta}(t)$. If we freeze the value of $\hat{\theta}(t)$ at its value at time t, the dynamics of the drive mass system can be described by $G(z, \theta^*)$ with $\theta^* = \hat{\theta}(t)$ (see (20)). The estimate $\hat{\omega}_{r,x}(t)$ of $\omega_{r,x}(t)$ at time t will be then chosen as the resonance frequency of the transfer function $G(z, \theta^*)$. To determine this resonance frequency in a computationally friendly way, we will use the following approach. Like the nominal model (2), $G(z, \theta^*)$ will be characterized by two complex poles and one real pole. Let us denote by p_{nom} one of the complex pole of the nominal model. This pole p_{nom} can be used to initialize a Newton-Raphson scheme aiming at determining the corresponding complex pole p^* of $G(z, \theta^*)$ (see e.g., [9]). Subsequently, using p^*, the following expression (approximately[15]) gives the resonance frequency of $G(z, \theta^*)$ i.e., $\hat{\omega}_{r,x}(t)$:

$$\hat{\omega}_{r,x}(t) = \frac{1}{T_s} \arg(p^*(t)) \tag{22}$$

where $\arg(p)$ denotes the argument of the complex number p.

The estimate $\hat{\omega}_{r,x}(t)$ obtained in this way can then be used to compute $x_{ref}(t)$ by using (15) with $\omega_{ref}(t) = \hat{\omega}_{r,x}(t)$. As a consequence, the scheme that we propose to tackle the variations of the resonance frequency of the drive mass system (when this system is operated with a linear controller) can be summarized by Figure 12.

Remark. Since the sampling time T_s used by the electronic card is small with respect to the expected variation of the resonance frequency, instead of updating the value of the resonance frequency at each sample t, one could further reduce the numerical complexity by updating the value of $\hat{\omega}_{r,x}(t)$ only every t_w samples i.e., the approach presented in this subsection to derive $\hat{\omega}_{r,x}(t)$ from $\hat{\theta}(t)$ will thus only be required once every t_w samples. This approach is moreover particularly interesting in combination with a recursive algorithm that is frequently re-initialized (see the previous subsection). Indeed, in the instants just after such a re-initialization, the estimate $\hat{\theta}(t)$ of $\theta_0(t)$ may be less accurate and so would be the estimate $\hat{\omega}_{r,x}(t)$ of $\omega_{r,x}(t)$ that could be deduced from that $\hat{\theta}(t)$. In the implementation of our algorithm, the recursive algorithm will be re-inialized every 30 seconds and the estimate $\hat{\omega}_{r,x}(t)$ of $\omega_{r,x}(t)$ will be determined 15 seconds after each re-initialization[16] and just before the next re-initialization. In other words, the signal $\hat{\omega}_{r,x}(t)$ that will be used to compute x_{ref} will have the form of a staircase signal with a (possible) step every 15 seconds.

4 Experimental results

In the previous section, we have presented our approach to improve the control of the drive mass system under varying resonance frequency circumstances. The resonance frequency of the drive

[15] This approximation is very accurate when the damping is very small as in the case considered in this work.

[16] The estimates $\hat{\theta}(t)$ and $\hat{\omega}_{r,x}(t)$ are indeed less accurate only for a few seconds.

mass system is estimated through a recursive identification algorithm and this estimate $\hat{\omega}_{r,x}(t)$ is used as $\omega_{ref}(t)$ in the expression (15) of the sinusoidal reference signal $x_{ref}(t)$ of the controller K_x (see Figure 12). This algorithm can be implemented in C++ in the electronic card of the platform AS3125-SDK that is used to instrument the MEMS gyroscope which is under consideration in the Next4MEMS project. The experimental setup is represented in Figure 13.

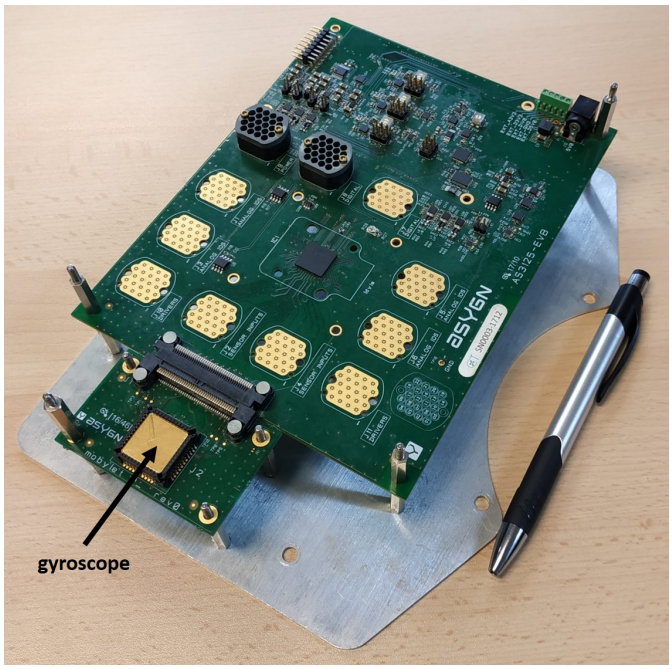

Figure 13: Picture of the experimental setup with the electronic card AS3125-SDK and the MEMS gyroscope.

Let us recall that the ambient temperature is the most important factor influencing the value of the resonance frequency. Consequently, in order to investigate the performance of our approach, we have operated the experimental setup presented in Figure 13 in a thermal chamber. Inside this chamber, the ambient temperature can be controlled and modified. In particular, we have subject the experimental setup to the temperature profile given in Figure 14. In this figure, we observe that the temperature, which is initially equal to 26 ^oC, is modified to a temperature of about 52 ^oC in approximately ten minutes and is subsequently kept (approximately) constant for another five minutes. Recall that the controller K_x has been designed based on a model identified at a nominal temperature of 30 ^oC.

Due to the modification of the temperature, the resonance frequency is modified and this fact is confirmed by the estimate $\hat{\omega}_{r,x}(t)$ of this resonance frequency that is computed every 15 seconds by the algorithm described in Section 3. This estimate is represented in Figure 15 and is compared to the resonance frequency $\omega_{r,x}^{nom}$ of the nominal model. We observe that, starting at[17] $\omega_{r,x}^{nom}$, the estimation algorithm requires approximately 45 seconds to settle. As we will see in the sequel, from that moment onwards, the control loop (see Figure 12) will have signals ϵ_x and u_x whose amplitudes are very close to the ones observed in Figure 6 (the so-called nominal performance that we want to maintain). Consequently, the estimate $\hat{\omega}_{r,x}(t)$ can be deemed close to the actual resonance frequency $\omega_{r,x}(t)$ of the drive mass system. Comparing the temperature profile of Figure 14 and

[17]Recall that the recursive identification algorithm is initialized at the nominal model.

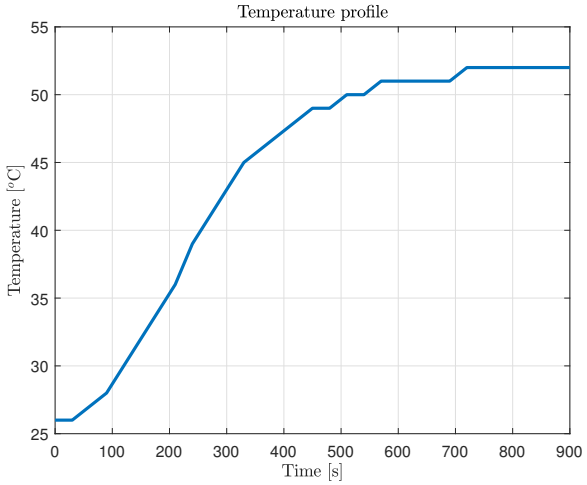

Figure 14: Temperature profile in the thermal chamber.

the resonance frequency profile of Figure 15, it is clear that the dynamics of the dependence of the resonance frequency on the temperature is rather complex.

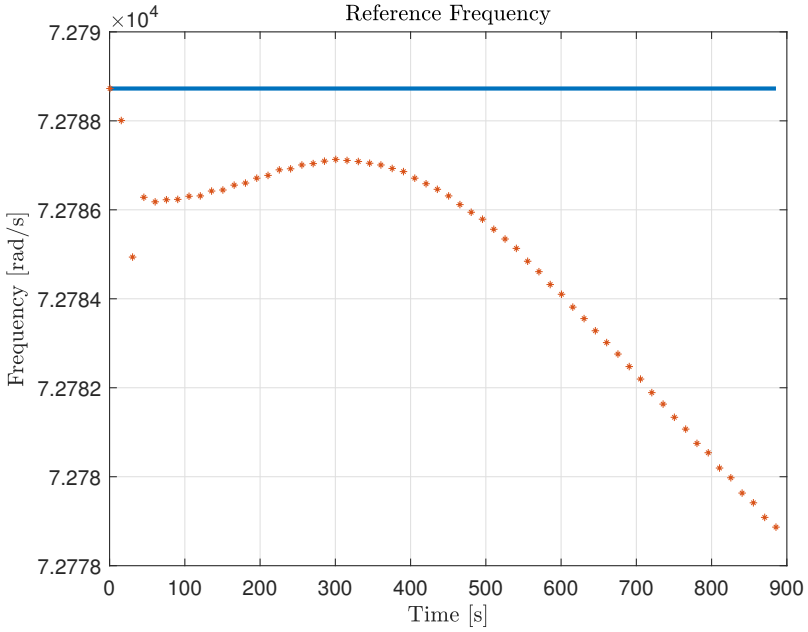

Figure 15: Estimate $\hat{\omega}_{r,x}(t)$ of the resonance frequency of the drive mass system (red asterisks) compared to the resonance frequency $\omega_{r,x}^{nom}$ of the nominal model (blue solid line)

The estimate $\hat{\omega}_{r,x}(t)$ of Figure 15 is used to compute the sinusoidal reference signal x_{ref} of the controller K_x as shown in Figure 12. Let us now see how this loop behaves by inspecting the control signal $u_x(t)$ and the tracking error signal $\epsilon_x(t)$. These signals are represented in Figure 16. During the 45 first seconds where x_{ref} is computed with a less accurate estimate of the resonance frequency (since the estimation algorithm is in its settling phase), we observe a large control effort[18]

[18]The control effort in fact hits the saturation during approximately 30 seconds.

and a large tracking error confirming the observations in Section 2.3 and confirming the need of constructing x_{ref} with a good estimate of the resonance frequency. After this settling phase, the signals $u_x(t)$ and $\epsilon_x(t)$ present amplitudes that are very close to the ones observed in the nominal case (see Figure 6). Note that the slight increase of the amplitude of ϵ_x (observed in Figure 8) is not visible here, but we observe a very small increase of the amplitude of u_x in the second part of the experiment. This may be due to the combination of, on the one hand, the very fast decrease of the resonance frequency in this part of the experiment (see Figure 15) and, on the other hand, the fact that $\hat{\omega}_{r,x}(t)$ is only updated every 15 seconds (see the remark at the end of Section 3).

The differences between the settling phase (where $\hat{\omega}_{r,x}(t)$ is less accurate) and the remaining of the experiment presented in Figure 16 clearly show the efficiency of our approach to deal with the adverse consequences of the variations of the resonance frequency when the drive mass system is controlled using an LTI controller (i.e., the control configuration used in the Next4MEMS project). In order to illustrate the benefit of our approach even further, let us perform a similar experiment in the thermal chamber without the adaptation of the reference signal x_{ref} i.e., x_{ref} is kept during the whole experiment equal to $x_{ref}(t) = 0.5\sin(\omega_{r,x}^{nom} t T_s)$ i.e., a sinusoid at the resonance frequency $\omega_{r,x}^{nom}$ of the nominal model. This leads to the signals ϵ_x and u_x given in Figure 17. It is clear that the control signal u_x observed in this figure is much larger that what is observed in Figure 16. This is particularly obvious in the second part of the experiment where the resonance frequency strongly varies (see Figure 15) and where u_x hits its saturation. This saturation of the control effort has a dramatic effect on the tracking error whose amplitude becomes almost as large as x_{ref}. Comparing Figures 16 and 17 clearly evidences the necessity of adapting x_{ref} to tackle the variations of the resonance frequency when the drive mass system is controlled using a LTI controller.

Remark. When facing resonance frequency variations such as the ones in Figure 15, the adaptation of x_{ref} proposed in this paper allows to maintain the (maximal) amplitudes of u_x and ϵ_x close to the ones observed in the nominal case (see Figure 6). Consequently, in order to tackle such resonance frequency variations, there seems to be no need of a more complex approach which, besides the adaptation of x_{ref}, would also involve the adaptation of K_x. If this would happen to be necessary in certain situations, let us however note that our recursive identification scheme would also enable the adaptation of K_x. The estimate $\hat{\theta}(t)$ could indeed be used as scheduling parameter in an Linear Parameter Varying controller [2, 20, 5]. Alternatively, as proposed in [17], one could also just use $\hat{\omega}_{r,x}(t)$ as scheduling parameter.

5 Conclusion

In a MEMS gyroscope, the proof mass of the drive mode (i.e., the drive mass system) must oscillate at its resonance frequency. When using a linear time-invariant controller to generate this oscillation, the variations of the resonance frequency (due e.g., to temperature variations) can severely alter the performance of the MEMS gyroscope. In this paper, we use recursive identification to estimate the dynamics of the drive mass system over time. Using this dynamics, we derive an estimate of the resonance frequency that is used to adapt the frequency of the sinusoidal reference signal that must be followed by the drive mass system. The experimental results show that the proposed approach allows to maintain a performance level that is very close to the nominal performance level even if the resonance frequency varies at a fast rate. By performance, we here mean the amplitudes of the tracking error and of the control actuation.

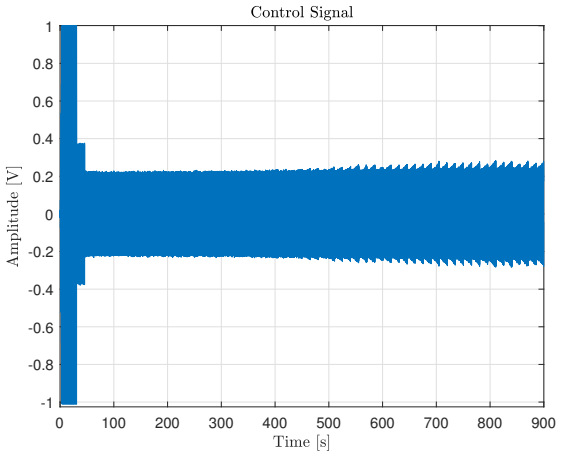

(a) u_x

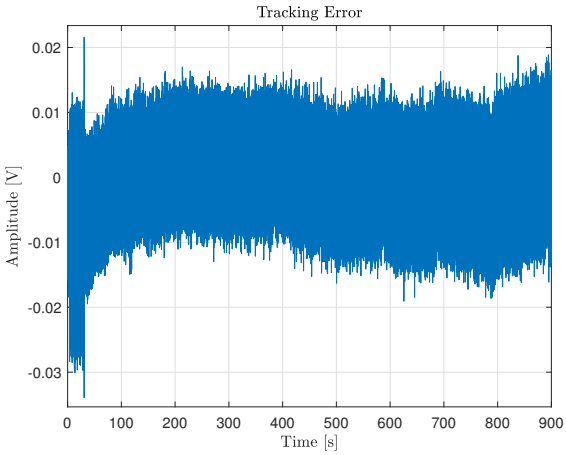

(b) ϵ_x

Figure 16: Results of the experiment where the setup is operated in a thermal chamber and where x_{ref} is adapted as shown in Figure 12.

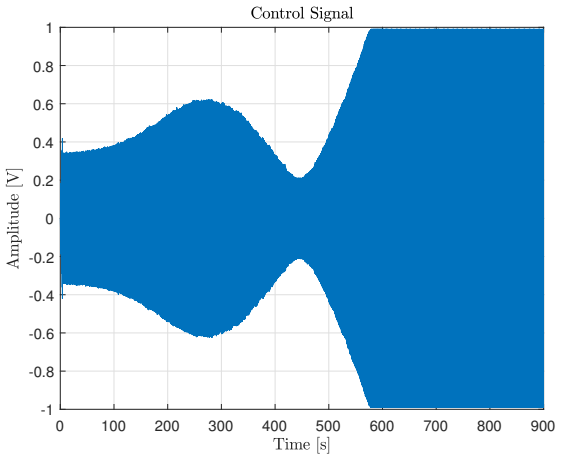

(a) u_x

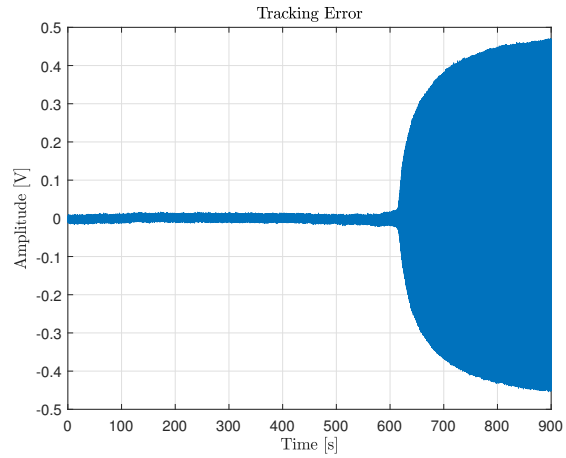

(b) ϵ_x

Figure 17: Results of the experiment where the setup is operated in a thermal chamber and where $x_{ref}(t) = 0.5\sin(\omega_{r,x}^{nom} t T_s)$.

References

[1] C. Acar and A. Shkel. *MEMS vibratory gyroscopes: structural approaches to improve robustness*. Springer Science & Business Media, 2008.

[2] P. Apkarian and P. Gahinet. A convex characterization of gain-scheduled H_∞ controllers. *IEEE Transactions on Automatic Control*, 40(5):853–864, 1995.

[3] Y-C Chen, R.T. M'Closkey, T.A. Tran, and B. Blaes. A control and signal processing integrated circuit for the JPL-boeing micromachined gyroscope. *IEEE Transactions on Control Systems Technology*, 13(2):286–300, 2005.

[4] K. Colin. *Data informativity for the Prediction Error Identification of MIMO Systems. Identification of a MEMS gyroscope.* PhD thesis, Ecole Centrale de Lyon, Université de Lyon, 2020. Available at https://tel.archives-ouvertes.fr/tel-03114994.

[5] M. Dinh, G. Scorletti, V. Fromion, and E. Magarotto. Parameter dependent H_∞ control by finite dimensional LMI optimization. *Int. J. Robust Nonlinear Control*, 15:383–406, 2005.

[6] L. Dong and D. Avanesian. Drive-mode control for vibrational MEMS gyroscopes. *IEEE transactions on industrial electronics*, 56(4):956–963, 2008.

[7] M. Egretzberger, F. Mair, and A. Kugi. Model-based control concepts for vibratory MEMS gyroscopes. *Mechatronics*, 22(3):241–250, 2012.

[8] J. Fei and C. Batur. Robust adaptive control for a MEMS vibratory gyroscope. *The International Journal of Advanced Manufacturing Technology*, 42(3):293–300, 2009.

[9] A. Gil, J. Segura, and N. Temme. *Numerical methods for special functions*. SIAM, 2007.

[10] V. Kempe. *Inertial MEMS: principles and practice*. Cambridge University Press, 2011.

[11] R. Leland. Adaptive control of a MEMS gyroscope using lyapunov methods. *IEEE Transactions on Control Systems Technology*, 14(2):278–283, 2006.

[12] L Ljung. *System Identification-Theory for the User 2nd edition, Prentice-Hall*. Upper Saddle River, USA, 1999.

[13] Lennart Ljung and Torsten Söderström. *Theory and practice of recursive identification*. MIT press, 1983.

[14] S. Park, R. Horowitz, S. Hong, and Y. Nam. Trajectory-switching algorithm for a MEMS gyroscope. *IEEE Transactions on Instrumentation and Measurement*, 56(6):2561–2569, 2007.

[15] M. Pishrobat and J. Keighobadi. Model predictive control of MEMS vibratory gyroscope. *IFAC Proceedings Volumes*, 47(3):7278–7283, 2014.

[16] F. Saggin. *Robust control for MEMS gyroscopes*. PhD thesis, Ecole Centrale de Lyon, Université de Lyon, 2021.

[17] F. Saggin, J. Ayala-Cuevas, A. Korniienko, and G. Scorletti. Parameter-dependent H_∞ control for MEMS gyroscopes: synthesis and analysis. *IFAC-PapersOnLine*, 53(2):7331–7337, 2020.

[18] F. Saggin, C. Pernin, A. Korniienko, G. Scorletti, and C. Le Blanc. Digital control of MEMS gyroscopes: a robust approach. In *2021 IEEE International Symposium on Inertial Sensors and Systems (INERTIAL)*, pages 1–4. IEEE, 2021.

[19] Mikko Saukoski. *System and circuit design for a capacitive MEMS gyroscope*. PhD thesis, Helsinki University of Technology, Faculty of Electronics, Communications and Automation, 2008.

[20] G. Scorletti and L. El Ghaoui. Improved LMI conditions for gain scheduling and related control problems. *International Journal of Robust and Nonlinear Control*, 8:845–877, 1998.

[21] D. Shaeffer. MEMS inertial sensors: a tutorial overview. *IEEE Communications Magazine*, 51(4):100–109, 2013.